# Shear-strain gradient induced polarization reversal in ferroelectric $BaTiO_3$ thin films: A first-principles total-energy study

Guannan Li,[1] Xiaokun Huang,[1] Jingsan Hu,[1] and Weiyi Zhang[1,2,*]

[1]*National Laboratory of Solid State Microstructures and Department of Physics, Nanjing University, Nanjing 210093, China*

[2]*Collaborative Innovation Center of Advanced Microstructures, Nanjing 210093, China*

(Received 5 December 2016; published 19 April 2017)

Based on the first-principles total-energy calculation, we have studied the shear-strain gradient effect on the polarization reversal of ferroelectric $BaTiO_3$ thin films. By calculating the energies of double-domain supercells for different electric polarization, shear-strain gradients, and domain-wall displacement, we extracted, in addition to the domain-wall energy, the polarization energy, elastic energy, and flexoelectric coefficient of a single domain. The constructed Landau-Devonshire phenomenological theory yields a critical shear-strain gradient of $9.091 \times 10^7$/m (or a curvature radius ($R$) of 110 Å) for reversing the 180° domain at room temperature, which is on the same order of the experimentally estimated value of $3.333 \times 10^7$/m ($R = 300$ Å). In contrast to the commonly used linear response theory, the flexoelectric coefficient derived from fitting the total energy to a Landau-Devonshire energy functional does not depend on the specific pseudopotential. Thus, our method offers an alternative numerical approach to study the flexoelectric effect.

DOI: 10.1103/PhysRevB.95.144111

## I. INTRODUCTION

Unlike the piezoelectric effect stipulating the relation between electric polarization ($P$) and mechanical strain ($e$) which appears only in space-inversion-symmetry–breaking crystals, the flexoelectric effect describes the dependence of electric polarization on inhomogeneous deformation (strain gradient), a phenomenon that is present universally in all kinds of materials irrespective of underlying symmetries. Therefore, the flexoelectric effect was not only observed in traditional inorganic crystals, but also in artificially structured materials and biological tissues [1]. It can be broadly applied in nanodevices such as sensors, actuators, and energy harvesters. The interest in flexoelectric effect arises, among other things, from the strain-gradient manipulation of electric polarization or even its reversal. This makes it possible to mechanically write and electrically read the ferroelectric memory bits. The flexoelectric effect was originally proposed by Kogan 50 years ago when he theoretically studied the induced electric polarization by inhomogeneous deformation [2]. This effect was confirmed experimentally by Scott 4 years later [3], and a reciprocal effect was also discovered by Bursian and Zaikovskii [4]. In these experiments, Scott found that surface strain gradient leads to the appearance of polar modes in centrosymmetric single crystals, while Bursian and co-workers observed an inhomogeneous deformation brought about by electric polarization. The flexoelectric effect has been overlooked for several decades because it is extremely small, and a large strain gradient is also difficult to achieve in macroscopic samples. The phenomenon has received renewed attention recently because a large strain gradient can be easily realized in nanoscaled ferroelectric structures and thus the flexoelectric effect is significantly enhanced.

In the past decade, great progress has been made regarding both the understanding of fundamental physics and the device applications of the flexoelectric effect [1]. On the experimental front, the flexoelectric effect has been investigated by several groups using different techniques such as substrate-induced bending [5–9], piezoelectric-force-microscope tip pressure (PFM) [10,11], and the cantilevel beam–based dynamical method [12]. Among others, Gruverman and co-workers [5] have studied the imprint behavior of ferroelectric $Pb(Zr,Ti)O_3$ capacitor thin films by bending the underlying Si substrate. Lu *et al.* [10] investigated the domain reversal of an ultrathin $BaTiO_3$ (BTO) ferroelectric film under the tip pressure of an atomic force microscope (AFM). They demonstrated the feasibility to write mechanically and read electrically the ferroelectric memory bits to avoid electric leakage and dielectric breakdown problems. Očenášek *et al.* [11] have shown that the flexoelectric domain switching is mainly driven by the shear-strain gradient. The flexoelectric coefficients have also been estimated to be the order of a few nC/m for bulk $BaTiO_3$ single crystals [9] instead of $\mu$ C/m suggested for ceramics samples [12]. The uncertainty in determining the flexoelectric coefficient was attributed to the reduced permittivity in thin films than that of bulk materials. The giant flexoelectric effect was also revealed through the hysteresis loop of ferroelectric $HoMnO_3$ thin films [8]. A strong flexoelectric effect was even observed in biological tissues [13] where the electric polarization was internally biased outward of the porcine aortic walls and the inward polarization is unstable. These experimental investigations have convincingly demonstrated that the flexoelectric effect can indeed be giant in ferroelectric nanomaterials, large enough to switch ferroelectric domains, or be applied in novel memory nanodevices.

Regarding the theoretical progress on flexoelectric effects, the flexoelectric coefficients were first estimated by Kogan from a phenomenological theory of simple dielectrics [2]. The distinction between piezoelectric and flexoelectric responses was clarified by Tagantsev using the classical ionic model [14]. A more quantitative analysis of the flexoelectric tensor has been made by Maranganti and Sharma [15] for ionic salts, perovskite dielectrics, and III-V and II-VI semiconductors using the lattice dynamics method. These previous studies mainly

*wyzhang@nju.edu.cn

 

concentrated on the ionic contribution and the electronic contribution to flexoelectric coefficients was not considered. The idea to compute the flexoelectric coefficient from a first-principles method was first formulated for element materials by Resta [16] in the framework of linear response theory and restricted to the longitudinal electronic contribution. The formulation was implemented by Hong and Vanderbilt [17] to calculate the flexoelectric coefficients of cubic insulating compounds. Since then, the formulism was refined by several research groups to address both the longitudinal and transverse strain gradients. Both ionic and electronic contributions are included [18–20]. However, the calculated flexoelectric coefficients are generally pseudopotential dependent and a correction with respect to the all-electron case is needed. Furthermore, transverse components require both charge and current response functions and are difficult to implement in practice [18].

A more direct approach to calculate the flexoelectric coefficient is to fix one type of atoms of compounds to simulate the strain gradient while computing the electric polarization change of relaxed structures at the position of maximal strain gradient using the first-principles method. With this method Hong *et al.* [21] computed the longitudinal flexoelectric coefficients of bulk ferroelectric $BaTiO_3$ and paraelectric $SrTiO_3$ compounds. Xu *et al.* calculated both the transverse and shear flexoelectric coefficients of bulk $BaTiO_3$ and $SrTiO_3$ [22]. Using the effective Hamiltonian technique, Ponomareva *et al.* [23] also computed the temperature dependence of flexoelectric coefficient of paraelectric $Ba_{1/2}Sr_{1/2}TiO_3$ thin films adopting a Monte Carlo simulation. All these works mainly focused on the dependence of electric polarization on local strain gradient in the paraelectric phase; the overall pattern of the energy functional on strain gradient and polarization was not systematically studied.

Clearly, having the accurate full energy functional is an important first step to discuss the polarization-reversal phenomena in inhomogeneously deformed ferroelectrics [5,11,12,24]. Previous studies concentrated most on the paraelectric phase; the nonlinear nature of the full energy functional on polarization was not considered. Most importantly, because the polarization definition is pseudopotential dependent, the accuracy of the flexoelectric coefficient is in doubt. These issues have to be dealt with consistently in order to give the precise information on the polarization reversal under strain gradient. Thus, to construct the true energy functional of deformed ferroelectrics, one has to compute the total energy of a ferroelectric for a given set of polarization ($P$), strain ($e$), and strain gradient ($\partial e/\partial x$). To avoid the pseudopotential dependence of polarization, we specify the structure with given polarization ($P$) with reference to the fully polarized bulk equilibrium structure at 0 K ($P_0$). To extract the flexoelectric coefficient, we consider a double-domain supercell with reversed polarizations and strain gradients so that the piezoelectric effect is absent. In this paper, we choose the tetragonal phase of ferroelectric $BaTiO_3$ compound as an example. The bulk flexoelectric coefficient is calculated using the first-principles total energy under pure shear-strain gradient. By fitting to the generalized Landau-Devonshire energy functional, we derived a whole set of parameters relating the electric polarization, strain, and strain gradient.

The rest of the paper is organized in the following way. In Sec. II, we first introduce the two-domain supercell model with sinusoidal shear-strain gradient. The local-density-approximation calculation as implemented in the Vienna *Ab Initio* Simulation Package (VASP), as well as the relevant parameter setting, are briefly described. In particular, the steps of the detailed fitting procedure to deduce the flexoelectric coefficient are outlined. In Sec. III, we present the numerical results on the cases of strain-free single-domain, strain-free double domain with domain wall, and the full double domain with a prescribed shear-strain gradient and electric polarization. The best fitting parameters and their relative errors are given in each step and discussed in comparison with available data from previous calculations or measurements. The obtained Landau-Devonshire energy functional for a single domain is then used to predict the polarization-reversal phenomena by shear-strain gradient and compared with the experimental measurement. The conclusions are drawn in Sec. IV.

## II. COMPUTATIONAL DETAILS

### A. Two-domain supercell with prescribed strain gradient and electric polarization

To facilitate the first-principles total-energy calculation, we construct the following two-domain supercell as illustrated in Fig. 1. The supercell consists of a $2Na \times b \times c$ $BaTiO_3$ unit cells with up-domain ($P$) and a down-domain ($-P$) of an $N$ unit cell each along the $a$ axis. $a$, $b$, and $c$ are the equilibrium lattice constants of the tetragonal phase of $BaTiO_3$. For the shear-strain-free case [see Fig. 1(a)], the theoretical atomic coordinates of bulk equilibrium ferroelectric $BaTiO_3$ at zero temperature are adopted for the fully polarized cases ($p = P/P_0 = \pm 1$, 180° domains) and those of the paraelectric cubic phase are used for the $p = 0$ case. The $z$ coordinates of the up-domain and down-domain are offset by $\Delta$ along the $c$ axis. $\Delta = 0$ for the paraelectric phase and has to be determined self-consistently for $p \neq 0$ cases. When a sinusoid shear strain is imposed along the $a$ axis [see Fig. 1(b)], both the up-domain and down-domain are under a similar pattern

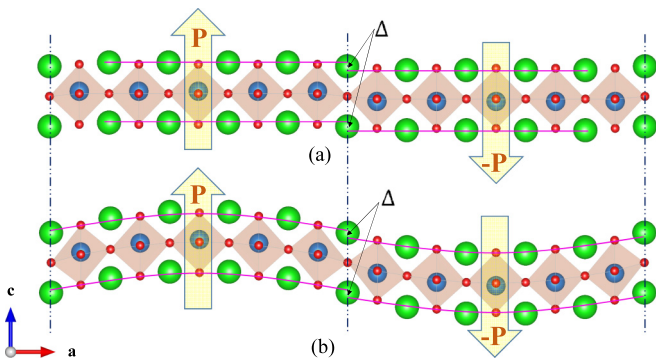


FIG. 1. Sketches of double-domain supercells. The supercell is composed of $2Na \times b \times c$ tetragonal $BaTiO_3$ unit cells with an up-domain ($p$) and a down-domain ($-p$) of $N$ unit cells each along $a$ axis. (a) Free-shear-strain case, and (b) with sinusoidal shear strain and strain gradient. Ba, Ti, and O atoms are represented as big green, middle light blue, and small red spheres, respectively.

of shear-strain gradient $\partial e_{31}/\partial x$. The shear strain in each domain is exactly compensated so that the piezoelectric effect is canceled precisely. Thus only the flexoelectric effect remains and can be deduced from the total-energy calculation. The configurations for other values of scaled polarization ($p$) can be interpolated from fully polarized and paraelectric phases.

The previous first-principles calculations showed that the width of a 180° domain wall in ferroelectric $BaTiO_3$ is very narrow and is about one lattice constant long [25,26]. In addition, the Ba-centered inversion symmetrical domain wall is energetically more favorable than a Ti-centered inversion symmetrical domain wall. Thus, we choose a Ba-centered inversion symmetrical domain wall in this paper. For a such narrow domain wall with prescribed shear-strain configuration in the bulk domain, the $z$ coordinate of the $i$th atom inside the supercell is given in terms of scaled modulation $h_0$:

$$z_i = \left(\bar{z}_i^0 + p\delta\bar{z}_i\right)c \pm 0.5pc\delta + (2Nc)h_0 \sin\left(\frac{2\pi x_i}{2Na}\right). \quad (1)$$

Here $\bar{z}_i^0$ are the scaled atomic coordinates of the paraelectric phase of $BaTiO_3$ in units of $c$ while $\delta\bar{z}_i$ are the corresponding scaled polar displacements of fully polarized bulk equilibrium $BaTiO_3$ in the absence of shear strain. $(\bar{x}^0,\bar{y}^0,\bar{z}^0)$ are (0.0,0.0,0.0) for Ba, (0.5,0.5,0.5) for Ti, (0.5,0.0,0.5) for $O_1$, (0.0,0.5,0.5) for $O_2$, and (0.5,0.5,0) for $O_3$, respectively. The up-domain and down-domain are offset by $\Delta = pc\delta$, which smoothly interpolates between the paraelectric and ferroelectric phases. The dimensionless parameter $\delta$ has to be determined by minimizing the domain-wall energy. The corresponding shear-strain configuration $e_{31}$ is

$$e_{31} = \frac{\partial z}{\partial x} = \left(\frac{2\pi c}{a}\right)h_0 \cos\left(\frac{2\pi x}{2Na}\right) \quad (2)$$

and the shear-strain-gradient configuration is

$$\frac{\partial e_{31}}{\partial x} = -\left(\frac{2\pi c}{a}\right)^2\left(\frac{h_0}{2Nc}\right)\sin\left(\frac{2\pi x}{2Na}\right). \quad (3)$$

In this way, the averaged shear strain and shear-strain gradient are given by $\sigma = \bar{e}_{31} = (2\pi c/a)(h_0/\sqrt{2})$ and $\eta = \partial\bar{e}_{31}/\partial x = (2\pi c/a)^2(h_0/2\sqrt{2}Nc) = 1/R$, respectively, and $R$ is the corresponding curvature radius. In our numerical calculations, we compute the total energy of a double-domain supercell for a given set of scaled polarization $p$, shear strain $\sigma$, shear-strain gradient $\eta$, and domain offset $\delta$ to sample the total-energy functional. Although the scaled atomic positions are fixed by the prescribed polarization, the total energy is optimized with respect to the lattice constants of the supercell.

### B. The total-energy calculations using density functional theory

With the double-domain supercell described above, the total energy of strained ferroelectric $BaTiO_3$ is calculated using a plane-waves basis with an energy cutoff of 500 eV and the projector-augmented-wave method as implemented in VASP [27]. The projector-augmented-wave potentials [28] include ten valence electrons for Ba ($5s^25p^66s^2$), 12 for Ti ($3s^23p^64s^23d^2$), and six for O ($2s^22p^4$). The exchange and correlation effects were described within the local density approximation (LDA) [29]. A $6\times6\times6$ Γ-centered $k$-point sampling is used for a single unit cell, and a $2\times6\times6$ Γ-centered $k$-point sampling for a supercell. The various $k$-point samplings have been well tested for structural and electronic convergences (see Supplemental Material [30]). Each self-consistent electronic calculation is converged to $10^{-6}$ eV and the tolerance force is set to 0.005 eV/Å for ionic relaxation. The ferroelectric polarization is calculated using the Berry phase approach for equilibrium tetragonal ferroelectric $BaTiO_3$ [31,32]. The pseudopotentials have also been first validated on the tetragonal phase of ferroelectric $BaTiO_3$. As shown in Table I, the obtained structural parameters are consistent with both the experimental measurements [33,34] and previous theoretical results [35]. The scaled atomic positions in the $P4mm$ space group provide the following ferroelectric displacements (assuming $\delta z_{Ba} \equiv 0$): $\delta z_{Ti} = +0.013$, $\delta z_{O_{1,2}} = -0.012$, and $\delta z_{O_3} = -0.019$. For the paraelectric cubic phase, the lattice constant $a = b = c = 3.950$ Å is obtained.

TABLE I. The structural parameters of tetragonal phase of ferroelectric $BaTiO_3$. $O_{1,2}$ and $O_3$ refer to the planar oxygens in $TiO_2$ and BaO planes. The scaled atomic $\bar{z}_i$ coordinates are in units of lattice constant $c$. The references where the data are cited are also indicated.

| | $\bar{z}_i$ (This work) | $\bar{z}_i$ (Experiment) | $\bar{z}_i$ (Theory) |
|---|---|---|---|
| $a$ (Å) | 3.941 | 3.991[a] | 3.943[c] |
| $c$ (Å) | 3.987 | 4.035[a] | 3.994[c] |
| $c/a$ | 1.012 | 1.011[a] | 1.013[c] |
| Ti | 0.487 | 0.489[a] | 0.492[c] |
| $O_{1,2}$ | 0.512 | 0.511[a] | 0.513[c] |
| $O_3$ | 0.019 | 0.018[a] | 0.021[c] |
| $P_0$ (C/m$^2$) | 0.251 | 0.260[b] | 0.229[c] |

[a]Reference [33].
[b]Reference [34].
[c]Reference [35].

Based on the structural parameters of the tetragonal phase of $BaTiO_3$, the supercell is constructed with $2Na\times b\times c$ unit cells stacked along the $a$ axis. For a given set of electric polarizations and a shear-strain-gradient configuration, the structural parameters of the supercell are optimized. To check the size effect on the Landau-Devonshire energy functional, the energy densities of the supercells with $N = 5,7,9$ are computed for comparison. It is found that the $N = 9$ case is already well converged; thus the discussion below focuses only on the $N = 9$ case.

### C. Fitting the total energy into Landau-Devonshire energy expansion

To extract the complete set of Landau-Devonshire parameters of the total energy calculated for various electric polarizations, shear strains, and shear-strain gradients, we divide the whole procedure into three steps:

(1) First, the total energy of single-domain ferroelectric $BaTiO_3$ is computed for various ferroelectric polarizations $0 \leqslant p \leqslant 1$. To eliminate the systematic error due to the size effect, we consider the supercell with $N$ unit cell stacked along the $a$ axis. For a given $p$, the atomic coordinates are obtained

by interpolation between the fully saturated ferroelectric phase and the paraelectric phase. Thus the total energy calculated this way should reproduce exactly those of the $p = 0$ and $p = 1$ cases. The evolutions of atomic configurations between these two extreme cases are difficult to figure out, and the configuration interpolation represents the best guess under current circumstances. According to Landau-Devonshire phenomenological theory, the polarization-dependent energy can be expanded into the following form:

$$E_1(P) = E(0) + (Nabc)E_P(P), \tag{4}$$

with

$$E_P(P) = a_1P^2 + a_2P^4 + a_3P^6 + a_4P^8. \tag{5}$$

Here $E(0)$ is the total energy of the supercell of the cubic paraelectric phase of $BaTiO_3$. $E_P(P)$ is the polarization-dependent Landau-Devonshire energy density expanded in Taylor series. $P = P_0p$ is the electric polarization, with $P_0 = 0.251$ C/m$^2$ denoting the saturated polarization at equilibrium. $a_1$, $a_2$, $a_3$, and $a_4$ are the dielectric stiffness and higher-order stiffness parameters. The $a_1$, $a_2$, $a_3$, and $a_4$ parameters are deduced from the best fit to Eqs. (4) and (5).

(2) In order to extract the energy density relevant to the flexoelectric effect, we first consider the strain-free double-domain supercell to identify the domain-wall energy density. The supercell consists of an up-domain ($p$) and a down-domain ($-p$) of $N$ unit cells, each along the $a$ axis [see Fig. 1(a)]. We chose a Ba-centered inversion symmetrical domain wall due to its low-domain-wall energy density. Because of the inverse flexoelectric effect, the mass centers of two domains are offset by a $pc\delta$ so that they are the same for the paraelectric phase [25]. $\delta$ has to be determined self-consistently for the $p \neq 0$ cases. Once the two-domain supercell is prescribed, the total energy $E_2(P,\delta)$ of the supercell can again be computed as a function of electric polarization $p$ and parameter $\delta$. After careful physical reasoning and tedious numerical trials, we find that the domain-wall energy $E_D(P,\delta)$ can be expanded into the following form after subtracting two single-domain energies:

$$E_2(P,\delta) = 2E(0) + 2(Nabc)E_P(P) + 2(bc)E_D(P,\delta) \tag{6}$$

with

$$E_D(P,\delta) = a_5P^2 + a_6P^4 + a_7P^6 + a_8P^2(\delta - \delta_0 - \delta_1p^2)^2. \tag{7}$$

The first three terms ($a_5$, $a_6$, $a_7$) refer to the domain-wall energy per unit area, while the last term ($a_8$) represents the energy penalty paid for domain-wall mismatch. As is obvious, the penalty energy vanishes for the paraelectric phase. The scaled optimal offset $\delta = \delta_0 + \delta_1p^2$ is obtained by the best fit to the domain-wall energy.

(3) Once the domain-wall energy is known as a function of electric polarization, we are able to focus on the flexoelectric effect. As we mentioned in the Introduction, for the sinusoidal strain configuration considered in this paper the piezoelectric effect is perfectly canceled due to the symmetrical strain distribution in each domain. The flexoelectric effect is left intact because the shear-strain gradient contributes coherently in both domains. To extract the flexoelectric parameter, we systematically computed the total energy $E_3(P,\sigma,\eta,\delta)$ of the supercell for various sets of electric polarization $P$, shear strain $\sigma$, shear-strain gradient $\eta$, and the dimensionless parameter $\delta$. Similarly, the known quantities from single domains, domain wall can be subtracted from the total energies so that the elastic and electromechanic coupling terms can be extracted:

$$\begin{aligned} &E_3(P,\sigma,\eta,\delta) \\ &\quad = 2E(0) + 2(Nabc)[E_P(P) + E_\sigma(\sigma) + E_{P\eta}(P,\eta)] \\ &\qquad + 2(bc)[E_D(P,\delta) + E_{D\eta}(P,\eta,\delta)], \end{aligned} \tag{8}$$

$$E_\sigma(\sigma) = a_9\sigma^2 + a_{10}\sigma^4, \tag{9}$$

$$E_{P\eta}(P,\eta) = a_{11}\eta P + a_{12}\eta P^3 + a_{13}\eta P^5 + a_{14}\eta^2P^2, \tag{10}$$

$$E_{D\eta}(P,\eta,\delta) = a_{15}\eta P(\delta - \delta_0 - \delta_1p^2). \tag{11}$$

Here $C_{44} = 2a_9$ is the bulk shear elastic constant, and $a_{10}$ is the high-order correction for elastic energy. $f_{1313} = 2a_{11}$ is the flexoelectric coefficient. $a_{12}$, $a_{13}$, and $a_{14}$ are the high-order corrections for the electromechanic coupling terms, while $a_{15}$ is the strain gradient domain-offset coupled energy. The strain-gradient square term is much smaller than the elastic energy term and can be extracted when different supercell sizes are fitted together [36]. It should be emphasized that high-order terms are small in comparison with quadratic terms and result from the high-order strain terms. In this way, the energy parameters for single domains, domain wall, and electromechanic coupling are identified and determined together with their relative standard deviations.

## III. RESULTS AND DISCUSSION

To investigate the shear-strain flexoelectric effect of bulk $BaTiO_3$, a comprehensive first-principles total-energy study has been carried out for a dense set of parameters of electric polarization ($P$), shear strain ($\sigma$), and shear-strain gradient ($\eta$) (see Supplemental Materials [30]). In the following, we analyze and discuss the numerical results and Landau-Devonshire energy fitting of supercell ($N = 9$) according to the major steps outlined in Sec. II.

For the shear-strain-free single-domain supercell, the polarization-dependent energy density $E_P(P)$ is plotted in Fig. 2. The empty circles are the calculated data points while the solid curve is the Landau-Devonshire energy fitting. The overall fitting is excellent and the fitting parameters are listed in Table II. Also listed are the previous experimentally estimated parameters deduced from phase transitions [37] and theoretically estimated parameters based on the lattice eigenvectors of paraelectric cubic phase and ferroelectric tetragonal phase [38]. Generally speaking, these parameters are rather scattered in values. Our estimated values are close to the cubic phase for $a_1$ and $a_2$ and to the tetragonal phase for $a_3$ and $a_4$. This result is understandable in view of the configuration interpolation used in our total-energy calculation [38]. As shown in Fig. 2, the polarization-dependent energy density shows a well-known symmetrical double-well structure with respect to the paraelectric phase. Although these values are computed at temperature $T = 0$ K, finite temperature $a_1(T)$

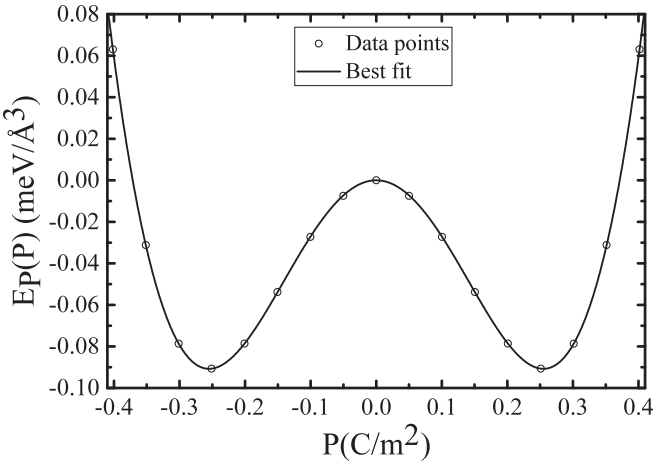


FIG. 2. The polarization-dependent energy density of single-domain $BaTiO_3$. The saturated polarization $P_0 = 0.251$ C/m$^2$ is set to that of the ferroelectric ground state. The circles are the calculated points, while the solid line represents the best fit by Eqs. (4) and (5).

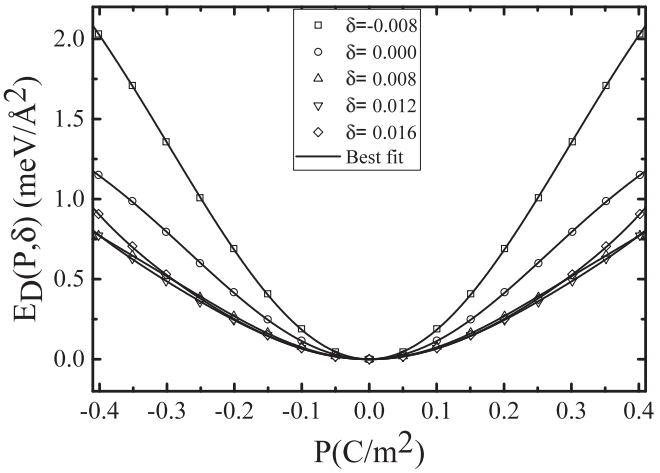


FIG. 3. The domain-wall energy densities as functions of electric polarization for different $\delta$. The symbols are the calculated points while solid lines represent the best fit by Eqs. (6) and (7). $\delta(p) = \delta_0 + \delta_1 p^2$ with $\delta_0 = 0.014\,2$ and $\delta_1 = -0.001\,6$.

can be approximated by $a_1(T)/a_1(0) = (1 - T/T_C)$, with $T_C$ denoting the Curie-Weiss temperature. As was customarily done, $a_2$, $a_3$, and $a_4$ are usually assumed to be temperature-independent quantities.

To prevent the domain-wall energy from interfering the extraction of the flexoelectric coefficient, we first identify the domain-wall energy from a shear-strain-free double-domain supercell. After subtracting the single-domain polarization energy from the total energy, the extracted domain-wall energies $E_D(P,\delta)$ are shown in Fig. 3 as functions of polarization $P$ and dimensionless offset parameter $\delta$. As expected, domain-wall energy shows a typical parabola shape with the best $\delta$ minimizing its energy. The optimized $\delta$ takes $\delta(p) = \delta_0 + \delta_1 p^2$, and the parameters $a_5$, $a_6$, $a_7$, and $a_8$ together best describe the functional form of the domain-wall energy density. The best fitting parameters are summarized in Table III. Note that the optimal domain offset for Ba, $\delta u_{\mathrm{Ba}} = (\delta_0 + \delta_1)c = 0.0126c$, is very close to the value for Pb, $\delta u_{Pb} = 0.010c$, in $PbTiO_3$ found by Meyer and Vanderbilt [26].

Now we are ready to address the elastic property and flexoelectric property under the sinusoidal shear-strain configuration. Since the piezoelectric effect is absent, only the flexoelectric effect remains. The elastic constant $C_{44}$, flexoelectric parameter $f_{1313}$, and the high-order parameters can be similarly deduced by best fitting Eqs. (8)–(11) and are listed in Table IV, together with the available experimental and theoretical data. Unlike the fitting procedures for single-domain and domain-wall energies where the relative errors are very small, the third fitting procedure inherited all the numerical inaccuracies from the first two steps. Thus the relative errors are significantly large. It should be mentioned that a large relative error for the parameter $a_{12}$ only indicates that this small term is probably irrelevant in the fitting. The obtained value $C_{44} = 1.2910 \times 10^{11}$ N/m$^2$ agrees well with the previous calculated value [39], being about twice the experimental measured value [40]. As shown in Table IV, the flexoelectric parameter $f_{1313} = 0.220$ V is smaller than the previous theoretical value, 0.85 V, of $BaTiO_3$ [22] and is comparable with the experimental value [1]. The high-order terms are generally small. They are mainly caused by the complex strain configuration, which deviates from the ideal model with only the strain and strain gradient. Thus, these high-order terms should be neglected when considering the phenomena originating from the flexoelectric effect.

In deriving the elastic and flexoelectric parameters outlined in step 3, the bulk strain-gradient square term $(a_{16}\eta^2)$ was not explicitly included in the Landau-Devonshire energy expansion [36]. For a single-size supercell, the elastic energy term $(a_9\sigma^2)$ and strain-gradient square term $(a_{16}\eta^2)$ are not separable because strain and strain gradient differ by a factor of $\pi/Na$ in our model strain configuration. They can be independently extracted when fitting simulation results for different supercell sizes together. Combining the energy data points for supercells $N = 7$ and $N = 9$, we obtain $a_{16} \approx 3.832 \times 10^{-10}$ N. Thus, the $a_{16}\eta^2$ term is much smaller than the $a_9\sigma^2$ term. For example, for a half cylinder with curvature

TABLE II. The Landau-Devonshire phenomenological parameters for single-domain $BaTiO_3$. The symbols $O$ and $T$ within the brackets denote the cubic and tetragonal phases of $BaTiO_3$.

| $a_i$ | This work | $\Delta a_i/a_i$ | Li *et al.* [37] | Ueda *et al.* [38] ($O$) | Ueda *et al.* [38] ($T$) | Units |
|---|---|---|---|---|---|---|
| $a_1$ | $-4.752 \times 10^8$ | 0.0003 | $-1.601 \times 10^8$ | $-7.430 \times 10^8$ | $-1.906 \times 10^9$ | V m/C |
| $a_2$ | $+4.347 \times 10^9$ | 0.0002 | $-2.097 \times 10^8$ | $+5.769 \times 10^9$ | $+1.183 \times 10^{10}$ | V m$^5$/C$^3$ |
| $a_3$ | $-8.048 \times 10^9$ | 0.0008 | $+1.294 \times 10^9$ | $-3.274 \times 10^9$ | $-1.218 \times 10^{10}$ | V m$^9$/C$^5$ |
| $a_4$ | $+1.100 \times 10^{10}$ | 0.0040 | $+3.863 \times 10^{10}$ | $+2.618 \times 10^9$ | $+1.832 \times 10^{10}$ | V m$^{13}$/C$^7$ |

TABLE III. The fitting parameters of domain-wall energy density.

| $a_i$ | $a_5$ | $a_6$ | $a_7$ | $a_8$ | $\delta_0$ | $\delta_1$ |
|---|---|---|---|---|---|---|
| Units | $\mathrm{V\,m^2/C}$ | $\mathrm{V\,m^6/C^3}$ | $\mathrm{V\,m^{10}/C^5}$ | $10^2\,\mathrm{V\,m^2/C}$ | | |
| | 0.1868 | –0.2821 | 0.5115 | 3.9404 | 0.0142 | –0.0016 |
| $\Delta a_i/a_i$ | 0.0035 | 0.0173 | 0.0646 | 0.0079 | | |

radius 110 Å, $a_{16}\eta^2/a_9\sigma^2 \approx 0.002\%$. However, including the $a_{16}\eta^2$ term affects the flexoelectric coefficient somewhat. The flexoelectric coefficient changes from 0.220 V without this term to 0.389 V with this term. This is so because the flexoelectric effect involves rather small energy and the size effect may play a role. Using Eq. (6.2.42) derived from the continuum phenomenological model in Ref. [25], the flexoelectric coefficient can also be estimated from the displacement of the mass centers of two domains across the domain wall, $f_{1313} = C_{44}\delta u/(2P_0) \approx 1.04$ V. This value is roughly 4 times the value $f_{1313} = 0.220$ V derived from the strained bulk domain and 3 times the value $f_{1313} = 0.389$ V when the strain-gradient square term is included. However, the rather small domain-wall width of 1–2 lattice constants can be one factor which makes the continuum model difficult to apply. The other factor can be attributed to the smallness of the flexoelectric term with regard to elastic and polarization terms.

Using the self-consistent fitting procedure outlined above, we are able to deduce the reliable Landau-Devonshire phenomenological parameters for single-domain $BaTiO_3$ as well as the elastic and flexoelectric parameters. The Landau-Devonshire energy functional, after dropping the high-order correction terms and domain-wall energy, can be written as follows:

$$E(P,\sigma,\eta) = a_1P^2 + a_2P^4 + a_3P^6 + a_4P^8 + (1/2)C_{44}\sigma^2 + (1/2)f_{1313}\eta P. \quad (12)$$

The constant energy term $E(0)$ is also removed for simplicity. To discuss the strain-gradient induced electric polarization reversal, the above energy functional has to be extended to finite temperature. As was customarily done, we assume $a_1(T)$ at finite temperature takes the form $a_1(T) = a_1[1 - (T/T_C)]$ and all other parameters are assumed to be temperature independent. Thus, the polarization-reversal phenomenon

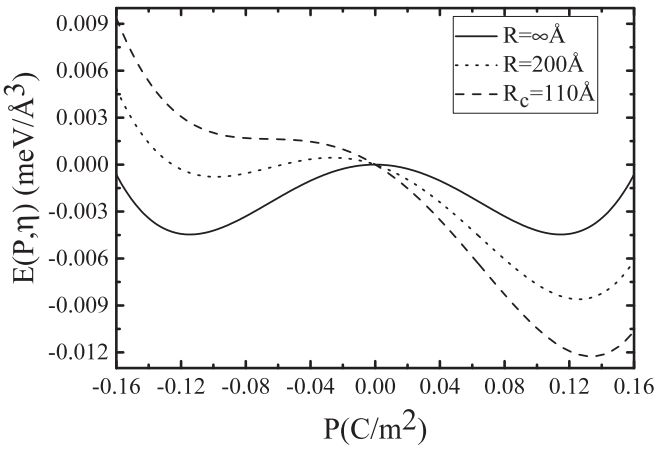


FIG. 4. The effect of shear-strain gradient on the polarization-dependent energy density of $BaTiO_3$ at $T = 300$ K ($T_C \approx 388$ K). The values of shear-strain gradient $\eta = 1/R$ are indicated by different line types.

essentially depends on two external variables, i.e., the experimental temperature $T$ and the strain gradient $\eta$ or curvature $R$. For ferroelectric $BaTiO_3$, the bulk Curie-Weiss temperature is $T_C = 388$ K (115 °C) [37]. We take $T = 300$ K for the experiments carried out at room temperature. However, it should be noted that our parameters are estimated for the bulk ferroelectric $BaTiO_3$, while polarization-reversal experiments are usually done on ferroelectric thin films. The parameters for bulk samples and thin films can differ from each other, in particular, the Curie-Weiss temperature can be significantly reduced with regard to bulk materials. To view the influence of shear-strain gradient $\eta$ on the polarization-dependent energy density, the Landau-Devonshire energy functional is plotted in Fig. 4 for $T/T_C = 0.773$ and for different values of the shear-strain gradient $\eta = 1/R$. In Fig. 4, the elastic energy is not included because it does not break the double-well symmetry of ferroelectric energy.

As shown in Fig. 4, the barrier height is reduced by 20 times while the optimized ferroelectric polarization is reduced by half at room temperature. The shear-strain gradient affects the energy profile in a similar way as an external electric field. Imposing a shear-strain gradient destroys the symmetrical double-well structure; the electric polarization is

TABLE IV. The elastic, flexoelectric, and high-order electromechanic coupling parameters of $BaTiO_3$.

| $a_i$ | This work | $\Delta a_i/a_i$ | Theory | Experiment | Units |
|---|---|---|---|---|---|
| $C_{44}$ | $+1.2910 \times 10^{+11}$ | 0.0007 | $+1.24 \times 10^{11}$[a] | $+0.611 \times 10^{11}$[b] | $\mathrm{N/m^2}$ |
| $a_{10}$ | $+0.2003 \times 10^{+11}$ | 0.3551 | | | $\mathrm{N/m^2}$ |
| $f_{1313}$ | +0.2200 | 0.1474 | ~0.85[c] | <0.15[d] | V |
| $a_{12}$ | -0.0182 | 7.5465 | | | $\mathrm{m^4\,V/C^2}$ |
| $a_{13}$ | +3.6583 | 0.2640 | | | $\mathrm{m^8\,V/C^4}$ |
| $a_{14}$ | $-7.6890 \times 10^{-9}$ | 0.0938 | | | $\mathrm{m^3\,V/C}$ |
| $a_{15}$ | $-0.3270 \times 10^{-6}$ | 0.0136 | | | V m |

[a]Reference [39].
[b]Reference [40].
[c]Reference [22].
[d]Reference [1].

more favored in one direction than the other. The domain-reversal barrier height shrinks as the shear-strain gradient increases and eventually vanishes at a critical shear-strain gradient $\eta_C$ or critical curvature radius $R_C$. If we used the bulk parameters of $BaTiO_3$ obtained in our first-principles calculations, $\eta_C \approx 9.091 \times 10^7/\text{m}$ ($R_C \approx 110$ Å). Comparing to the experimentally observed value $\eta_C \approx 3.333 \times 10^7/\text{m}$ ($R_C \approx 300$ Å) [11], the theoretically estimated value has the same order of magnitude but is 3 times smaller than the experimentally suggested one. The following reasons may affect the theoretical prediction: (1) The Curie-Weiss temperature of thin ferroelectric films is significantly reduced in comparison with that of bulk $BaTiO_3$. For example, the Curie-Weiss temperature for ferroelectric 35-nm thin film of $BaTiO_3$ is reduced to $T_C \approx 337$ K [41] and yields $\eta_C \approx 3.125 \times 10^7/\text{m}$ or $R_C \approx 320$ Å, which is very close to the experimentally measured value. (2) At finite temperature, the stabilities of up- and down-domains are not determined by the internal energy but rather by the Helmholtz free energy. The thermal fluctuation is important and makes the polarization reversal easier at finite temperature. (3) In domain-reversal experiments, the shear, transverse, and longitudinal flexoelectricities act in a coherent fashion: this further enriches the paths of phase transition. (4) For the finite-size ferroelectric thin films, the boundary effect and surface piezoelectric effect may decrease the effective susceptibility, thus enhancing the effective flexoelectricity [9].

## IV. CONCLUSION

In summary, the elastic, flexoelectric, and parameters of Landau-Devonshire polarization-dependent energy density are obtained by best fitting the first-principles total energy for different polarization, shear-strain, and shear-strain-gradient configurations of $BaTiO_3$. In order to extract the flexoelectric parameter unambiguously, we divide the numerical procedure into three controllable steps: (1) the Landau-Devonshire parameters are first obtained from a single-domain ferroelectric $BaTiO_3$; (2) the parameters of domain-wall energy are deducted from a shear-strain-free 180° double-domain structure after subtracting the single-domain contribution; and (3) the parameters of elastic, flexoelectric, and high-order correction terms are derived from the double-domain structure with a sinusoidal shear-strain pattern. The extracted elastic coefficient is in excellent agreement with previous theoretical values and is comparable with experimental measurement. In this way we constructed the Landau-Devonshire energy functional with given electric polarization, shear strain, and shear-strain gradient. Then we applied the Landau-Devonshire energy functional to study the shear-strain gradient induced polarization reversal in ferroelectric $BaTiO_3$ thin films. Our computed flexoelectric parameter $f_{3131} = 0.220$ V yields a critical curvature radius of $R_C = 110$ Å, which is on the same order of magnitude as the measured one ($R_C = 300$ Å). The possible reasons for discrepancy are also discussed. It should be emphasized that our flexoelectric coefficient is obtained from best fitting to the first-principles calculated total energy. The obtained coefficient is not limited to small polarization and does not sensitively depend on the adopted pseudopotential. Therefore, our method offers an alternative numerical approach to compute the flexoelectric property as well as domain-reversal phenomena.

## ACKNOWLEDGMENTS

This work was supported in part by the National Natural Science Foundation of China (Grant No. 11474148). We also thank the High Performance Computing Center of Nanjing University for part of the numerical calculations.

[1] P. Zubko, G. Catalan, and A. K. Tagantsev, Annu. Rev. Mater. Res. **43**, 387 (2013).
[2] S. M. Kogan, Sov. Phys. Solid State **5**, 2069 (1964).
[3] J. F. Scott, J. Chem. Phys. **48**, 874 (1968).
[4] É. V. Bursian and O. I. Zaikovskii, Sov. Phys. Solid State **10**, 1121 (1968).
[5] A. Gruverman, B. J. Rodriguez, A. I. Kingon, R. J. Nemanich, and A. K. Tagantsev, Appl. Phys. Lett. **83**, 728 (2003).
[6] P. Zubko, G. Catalan, A. Buckley, P. R. L. Welche, and J. F. Scott, Phys. Rev. Lett. **99**, 167601 (2007).
[7] G. Catalan, A. Lubk, A. H. G. Vlooswijk, E. Snoeck, C. Magen, A. Janssens, G. Rispens, G. Rijnders, D. H. A. Blank, and B. Noheda, Nat. Mater. **10**, 963 (2011).
[8] D. Lee, A. Yoon, S. Y. Jang, J.-G. Yoon, J.-S. Chung, M. Kim, J. F. Scott, and T. W. Noh, Phys. Rev. Lett. **107**, 057602 (2011).
[9] J. Narvaez, S. Saremi, J. W. Hong, M. Stengel, and G. Catalan, Phys. Rev. Lett. **115**, 037601 (2015).
[10] H. Lu, C.-W. Bark, D. Esque de los Ojos, J. Alcala, C. B. Eom, G. Catalan, and A. Gruverman, Science **336**, 59 (2012).
[11] J. Očenášek, H. Lu, C.-W. Bark, C. B. Eom, J. Alcalá, G. Catalan, and A. Gruverman, Phys. Rev. B **92**, 035417 (2015).
[12] W. Ma and L. E. Cross, Appl. Phys. Lett. **88**, 232902 (2006).
[13] Y. M. Liu, Y. H. Zhang, M.-J. Chow, Q. N. Chen, and J. Y. Li, Phys. Rev. Lett. **108**, 078103 (2012).
[14] A. K. Tagantsev, Phys. Rev. B **34**, 5883 (1986).
[15] R. Maranganti and P. Sharma, Phys. Rev. B **80**, 054109 (2009).
[16] R. Resta, Phys. Rev. Lett. **105**, 127601 (2010).
[17] J. Hong and D. Vanderbilt, Phys. Rev. B **84**, 180101 (2011).
[18] J. Hong and D. Vanderbilt, Phys. Rev. B **88**, 174107 (2013).
[19] M. Stengel, Phys. Rev. B **88**, 174106 (2013).
[20] M. Stengel, Nat. Commun. **4**, 3693 (2013).
[21] J. Hong, G. Catalan, J. F. Scott, and E. Artacho, J. Phys.: Condens. Matter **22**, 112201 (2010).
[22] T. Xu, J. Wang, T. Shimada, and T. Kitamura, J. Phys.: Condens. Matter **25**, 415901 (2013).
[23] I. Ponomareva, A. K. Tagantsev, and L. Bellaiche, Phys. Rev. B **85**, 104101 (2012).
[24] Y. J. Gu, Z. J. Hong, J. Britson, and L.-Q. Chen, Appl. Phys. Lett. **106**, 022904 (2015).
[25] See Eq. (6.2.42) at page 304 and Table 6.3.1 on page 317, A. K. Tagantsev, L. E. Cross, and J. Fousek, *Domains in Ferroic Crystals and Thin Films* (Springer, Dordrecht, 2010).

[26] B. Meyer and D. Vanderbilt, Phys. Rev. B **65**, 104111 (2002).
[27] G. Kresse and J. Furthmüller, Phys. Rev. B **54**, 11169 (1996).
[28] P. E. Blöchl, Phys. Rev. B **50**, 17953 (1994).
[29] J. P. Perdew and Y. Wang, Phys. Rev. B **45**, 13244 (1992).
[30] See Supplemental Material at http://link.aps.org/supplemental/10.1103/PhysRevB.95.144111 for structural and electronic convergences.
[31] R. D. King-Smith and D. Vanderbilt, Phys. Rev. B **47**, 1651 (1993).
[32] R. Resta, Rev. Mod. Phys. **66**, 899 (1994).
[33] T. Toshio, K.-H. Hellwege, H. Landolt, R. Börnstein, and O. Madelung, in *Ferro- and Antiferroelectric Substances*, edited by K.-H. Hellwege and A. M. Hellwege, Landolt-Börnstein (Springer-Verlag, Berlin, 1981), Group III, Vol. 3.
[34] H. H. Wieder, Phys. Rev. **99**, 1161 (1955).
[35] M. Fechner, S. Ostanin, and I. Mertig, Phys. Rev. B **77**, 094112 (2008).
[36] A. N. Morozovska, E. A. Eliseev, C. M. Scherbakov, and Y. M. Vysochanskii, Phys. Rev. B **94**, 174112 (2016).
[37] Y. L. Li, L. E. Cross, and L.-Q. Chen, J. Appl. Phys. **98**, 64101 (2005).
[38] M. Ueda and K. Miura, Jpn. J. Appl. Phys. (1962–1981) **53**, 05FE04 (2014).
[39] J. J. Wang, F. Y. Meng, X. Q. Ma, M. X. Xu, and L. Q. Chen, J. Appl. Phys. **108**, 034107 (2010).
[40] M. Zgonik, P. Bernasconi, M. Duelli, R. Schlesser, P. Günter, M. H. Garrett, D. Rytz, Y. Zhu, and X. Wu, Phys. Rev. B **50**, 5941 (1994).
[41] G. F. Huang and S. Berger, J. Appl. Phys. **93**, 2855 (2003).